ARTICLE

Tough Germanium Nanoparticles under Electrochemical Cycling

Wentao Liang,[†] Hui Yang,[†] Feifei Fan,[‡] Yang Liu,[§] Xiao Hua Liu,[§] Jian Yu Huang,[§] Ting Zhu,[‡,*] and Sulin Zhang[†,*]

[†]Department of Engineering Science and Mechanics, The Pennsylvania State University, University Park, Pennsylvania 16802, United States, [‡]Woodru School of Mechanical Engineering, Georgia Institute of Technology, Atlanta, Georgia 30332, United States, and [§]Center for Integrated Nanotechnologies (CINT), Sandia National Laboratories, Albuquerque, New Mexico 87185, United States

ABSTRACT Mechanical degradation of the electrode materials during electrochemical cycling remains a serious issue that critically limits the capacity retention and cyclability of rechargeable lithium-ion batteries. Here we report the highly reversible expansion and contraction of germanium nanoparticles under lithiation delithiation cycling with *in situ* transmission electron microscopy (TEM). During multiple cycles to the full capacity, the germanium nanoparticles remained robust without any visible cracking despite 260% volume changes, in contrast to the size-dependent fracture of silicon nanoparticles upon the first lithiation. The comparative *in situ* TEM study of fragile silicon nanoparticles suggests that the tough behavior of germanium nanoparticles can be attributed to the weak anisotropy of the lithiation strain at the reaction front. The tough germanium nanoparticles offer substantial potential for the development of durable, high-capacity, and high-rate anodes for advanced lithium-ion batteries.

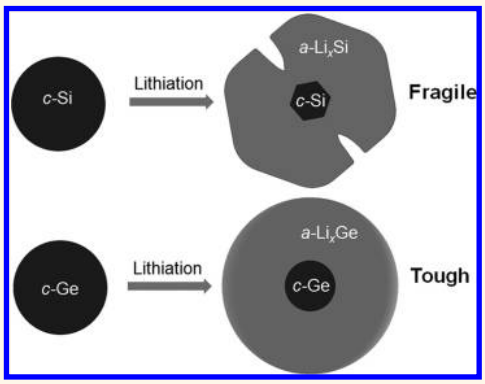

KEYWORDS: lithium-ion battery · fracture · anisotropic lithiation strain · *in situ* transmission electron microscopy

The development of advanced lithium-ion batteries requires new electrode materials with superior energy density, power density, and cyclability.[1−3] Mechanical degradation of the electrode materials during electrochemical cycling remains a serious issue[4−13] that critically limits the cycle life of lithium-ion batteries. Silicon (Si) is being considered as the next-generation anode material due to its high lithium (Li) capacity (3579 mAhg^{-1}),[14] more than an order of magnitude higher than the carbonaceous materials (372 mAhg^{-1}) currently used in Li-ion batteries. However, during electrochemical lithiation, Si electrodes undergo large and anisotropic expansion up to 280%, leading to fracture and capacity loss even in the first cycle.[4−13] Germanium (Ge), a group IV element as carbon and Si, has thus far received less attention. Several unique characteristics position Ge as a promising anode material. It possesses a high capacity (1384 mAhg^{-1}).[15] Both the electronic conductivity of Ge and the Li diffusivity within Ge are much higher than those in Si,[16,17] thereby enabling the high-rate performance of Ge electrodes. Despite these favorable properties and recent experiments showing the high performance of Ge-based anodes,[18−21] the capacity retention and cyclability of Ge electrodes, which are major concerns for high-capacity anodes, remain unclear.

Here we report the highly reversible expansion and contraction of germanium nanoparticles (GeNPs) under electrochemical cycling using *in situ* transmission electron microscopy (TEM). Our results revealed that during multiple lithiation delithiation cycles GeNPs of a large size range (from 100 nm to submicrometer) remained robust without any visible cracking despite 260% volume changes. This is in stark contrast to the size-dependent fracture of silicon nanoparticles (SiNPs) upon the first lithiation.[7] We further conducted the *in situ* TEM study, supported by the chemomechanical modeling, to reveal the strong crystallographic orientation effect on fracture in fragile SiNPs. On this basis, we attribute the tough behavior of GeNPs to the weak anisotropy of the lithiation strain at the reaction front (*i.e.*, the phase boundary between

* Address correspondence to suz10@psu.edu, ting.zhu@me.gatech.edu.

Received for review January 21, 2013 and accepted March 4, 2013.

Published online 10.1021/nn400330h

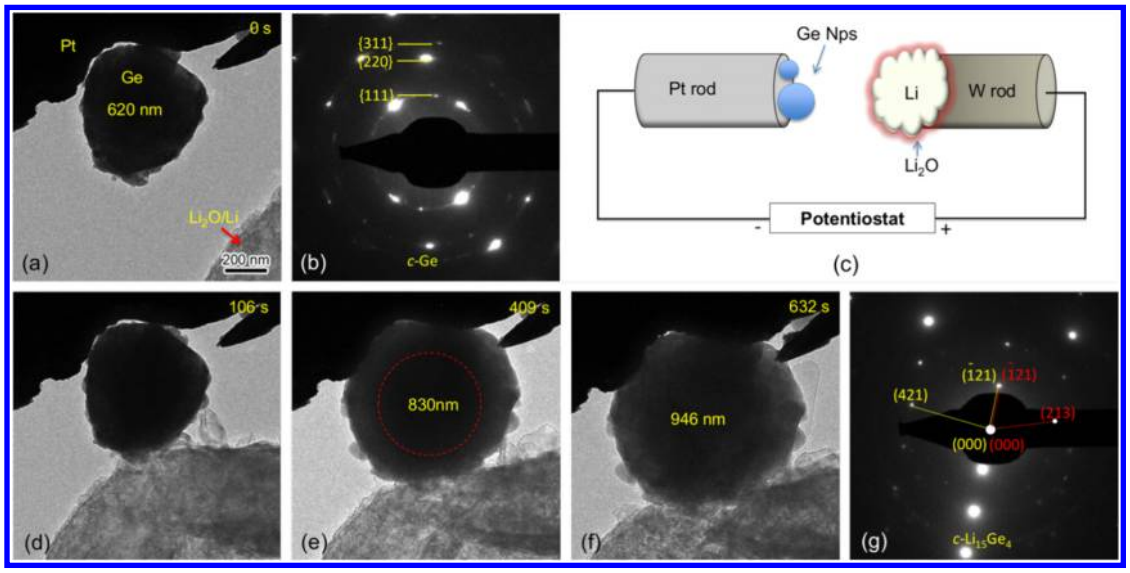

Figure 1. Morphological evolution and phase transformation in a *c*-GeNP during lithiation. (a) Pristine *c*-GeNP with a diameter of 620 nm. (b) EDP indicates that the GeNP is single-crystalline. (c) Schematic illustration of the *in situ* nanobattery setup, consisting of a single GeNP as the working electrode, bulk Li metal as the counter electrode, and a naturally grown Li_2O surface layer as the solid electrolyte. (d f) TEM snapshots showing the morphological evolution and uniform volume expansion of the GeNP upon lithiation. (d) Pristine GeNP was brought into contact with the Li_2O/Li electrode. (e) Lithiation-induced crystal-to-amorphous phase transformation, forming the structure with a crystalline core and an amorphous shell. The amorphous crystalline interface is marked by the red dashed circle. (f) *c*-$Li_{15}Ge_4$ phase formed after full lithiation to *a*-$Li_{15}Ge_4$, as indicated by the EDP shown in (g).

the amorphous shell and crystalline core), which correlates with its nearly crystallographic orientation-independent mobility.[22 25] The lithiation isotropy mitigates the buildup of high, non-uniform stresses, presenting a novel mechanism of averting the fracture in high-capacity electrodes.

RESULTS AND DISCUSSION

GeNPs were prepared by grinding a Ge wafer for 30 min. The ground Ge powders were then dispersed in ethanol solution, followed by ultrasonic treatment. A tip-flattened Pt rod was dipped into the solution. GeNPs were attached onto the end of the Pt rod. Figure 1a shows a typical pristine GeNP with a diameter of 620 nm. The electron diffraction pattern (EDP) in Figure 1b indicates that the as-prepared GeNP was single-crystalline, denoted as *c*-GeNP. To study the lithiation delithiation cycling behavior of GeNPs, an electrochemical device suited for *in situ* TEM experiment was constructed, as schematically shown in Figure 1c. The device consisted of three essential components: a single GeNP as the working electrode sitting on a Pt rod, a small piece of bulk Li metal as the counter electrode, and a native Li_2O surface layer on the Li metal as the solid electrolyte. All of the electrochemical tests were conducted in a Tecnai F-30 HRTEM with a Nanofactory TEM scanning tunneling microscopy (STM) holder. The *in situ* TEM study enables the real-time imaging of electrochemical reactions in GeNPs during the lithiation delithiation cycling.[6,22,26 29]

Figure 1d f shows the morphological evolution and phase transformation of an individual *c*-GeNP. To initiate the lithiation, a bias potential of 2 V was applied to the *c*-GeNP with respect to a Li metal electrode. The entire surface of the GeNP was quickly covered by Li ions, due to their much higher diffusion rate on the surface than in the bulk of Ge, similar to Si.[7] At 106 s (Figure 1d), the GeNP began to expand, indicative of the start of bulk lithiation. As the lithiation proceeded (see Figure 1e), Li flowed nearly uniformly from the surface to the center of the GeNP along the radial direction, forming the structure with a core of *c*-Ge and a lithiated shell of amorphous Li_xGe (*a*-Li_xGe). The similar core shell mode of lithiation was also observed in crystalline Si nanowires (*c*-SiNWs)[6,28] and Si nanoparticles (*c*-SiNPs).[7] Figure 1e shows that the lithiated GeNP expanded in a nearly isotropic manner to 830 nm. The isotropy of lithiation can be clearly seen from the approximately uniform thickness of the amorphous shell, where the core shell interface is marked by the red dashed circle. At 632 s, the GeNP was fully lithiated (Figure 1f) and its diameter increased to 946 nm, which corresponds to 260% volume increase, consistent with the 280% volume increase of the fully lithiated SiNPs (*a*-$Li_{15}Si_4$).[7,30] The lithiated GeNP consisted of the *a*-$Li_{15}Ge_4$ phase, which was subsequently crystallized to *c*-$Li_{15}Ge_4$,[31,32] as identified by the EDP in Figure 1g. The crystallization of *a*-Li_xGe to *c*-$Li_{15}Ge_4$ was a simultaneous process for the whole nanoparticle without any phase boundary observed, which is similar to the congruent

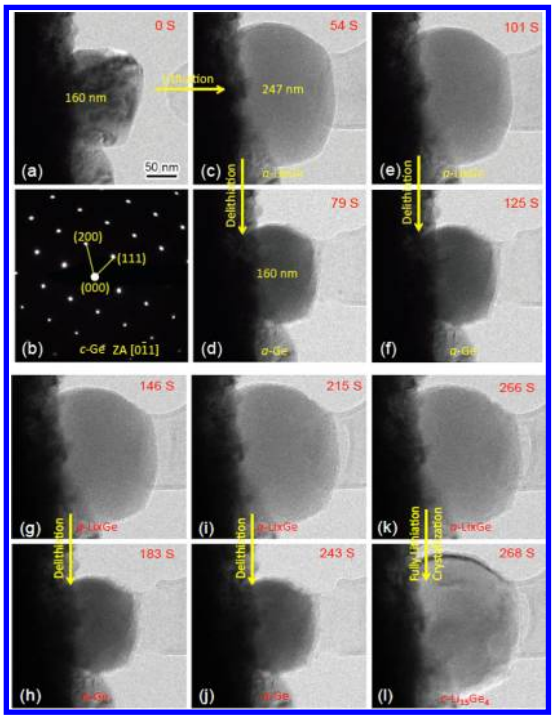

Figure 2. Multicycling of a single *c*-GeNP. (a) Pristine GeNP with a nearly spherical shape is 160 nm in diameter. (b) EDP of the pristine GeNP indicates that the nanoparticle is single-crystalline. (c,d) First lithiation delithiation cycle. A bias of 1 V was applied in the lithiation process. The diameter increased to 247 nm with *a*-Li_xGe formed. Then, a bias of 1 V was applied to initiate delithiation. The *a*-Ge phase formed, and the diameter decreased to 160 nm after full delithiation. (e j) Second, third, and fourth lithiation delithiation cycles showing the same behavior as the first cycle, demonstrating the cyclability of the GeNP. (k,l) Fifth lithiation and crystallization. The *a*-Li_xGe phase formed and then crystallized to *c*-$Li_{15}Ge_4$.

crystallization of *a*-Li_xSi.[32] The two-step phase transformation of *c*-Ge → *a*-Li_xGe → *c*-$Li_{15}Ge_4$ is consistent with the previous study of lithiation in *c*-GeNWs.[22] However, the lithiated GeNP did not fracture even though its initial size was considerably large, in contrast to the *c*-SiNPs that typically fracture into pieces upon lithiation provided that the initial diameter exceeds 150 nm.[7]

We next examine the cycling behavior of GeNPs. A *c*-GeNP with a nearly spherical shape and initial diameter of 160 nm was selected, as shown in Figure 2a. The corresponding EDP is given in Figure 2b, confirming its single-crystalline phase. A bias of 1 V was applied to this GeNP. After 54 s, the *c*-GeNP was fully lithiated to *a*-$Li_{15}Ge_4$ (Figure 2c) and its diameter increased to 247 nm, corresponding to 260% volume increase. Then the potential was reversed to 1 V before crystallization occurred. The spherical *a*-Li_xGe NP shrunk instantly in a uniform manner and was fully delithiated to its original size of 160 nm (Figure 2d), which suggested that the Li ions had been completely extracted from the *a*-$Li_{15}Ge_4$ NP. The fully delithiated phase was identified as *a*-Ge, as examined in detail later. After the first cycle, repeated lithiation delithiation between *a*-Ge and *a*-Li_xGe was conducted by periodically reversing the applied potential, as shown in Figure 2e k and the videos in the Supporting Information. It is noted that once the GeNP was fully lithiated to *a*-$Li_{15}Ge_4$, the applied potential should be reversed immediately before *a*-$Li_{15}Ge_4$ crystallized. Such immediate potential reversal was crucial in order to further delithiate the *a*-Li_xGe NP. In contrast, the applied potential was intentionally held for a relatively long time during the lithiation stage at the fifth cycle (Figure 2l), so as for *a*-Li_xGe to crystallize to *c*-$Li_{15}Ge_4$. After crystallization, the *c*-$Li_{15}Ge_4$ phase could no longer be delithiated even with a higher reverse potential (2 V). The inability of delithiation was manifested by the nearly constant volume before and after the reverse potential was applied, indicating a high affinity of Li with Ge in the *c*-$Li_{15}Ge_4$ phase.

To demonstrate the controlled formation of various crystalline and amorphous phases during lithiation delithiation cycling, we conducted a separate test for a *c*-GeNP with an initial diameter of 160 nm, as shown in Figure 3a. The pristine GeNP was single-crystalline, as shown by the EDP in Figure 3b. A bias of 1 V was applied to the *c*-GeNP with respect to the Li metal electrode. After 155 s, the *c*-GeNP was partially lithiated and the amorphous *a*-Li_xGe phase formed (Figure 3c) in the lithiated shell. The corresponding EDP of *a*-Li_xGe is shown in Figure 3d, consistent with the EDP previously observed in lithiated GeNWs. Before *a*-Li_xGe crystallized, the potential was reversed to 1 V. The extraction of Li ions from the *a*-Li_xGe phase resulted in the formation of the *a*-Ge phase (Figure 3e), as confirmed by the EDP in Figure 3f. During the second cycle, *a*-GeNP was initially lithiated to *a*-Li_xGe, then crystallized to *c*-$Li_{15}Ge_4$ (Figure 3g with the corresponding EDP in Figure 3h) under a prolonged holding of the applied voltage.

The above experiments demonstrated that, despite the large volume changes during electrochemical cycling, the GeNPs appeared to be unexpectedly tough, in contrast to the fragility (*i.e.*, ease of fracture) of SiNPs.[7,33] This motivated a comparative study of the lithiation behaviors of Si and Ge, which differ in several key aspects. First, the lithiation-induced swelling in *c*-GeNPs was nearly isotropic, in contrast to the strong anisotropic swelling in *c*-SiNPs and *c*-SiNWs.[6,7,28] Recent studies showed that the apparent swelling behavior in *c*-Si and *c*-Ge, both of which undergo the two-phase lithiation, is critically governed by the reaction (including rate and expansion) at the two-phase boundary, that is, the sharp interface between the crystalline core and amorphous shell.[13,34] The isotropic swelling in lithiated GeNPs suggests that the Li Ge reaction rate at the lithiation reaction front is insensitive to the crystallographic orientation of the phase boundary in GeNPs. In Figure 4, we compare the typical

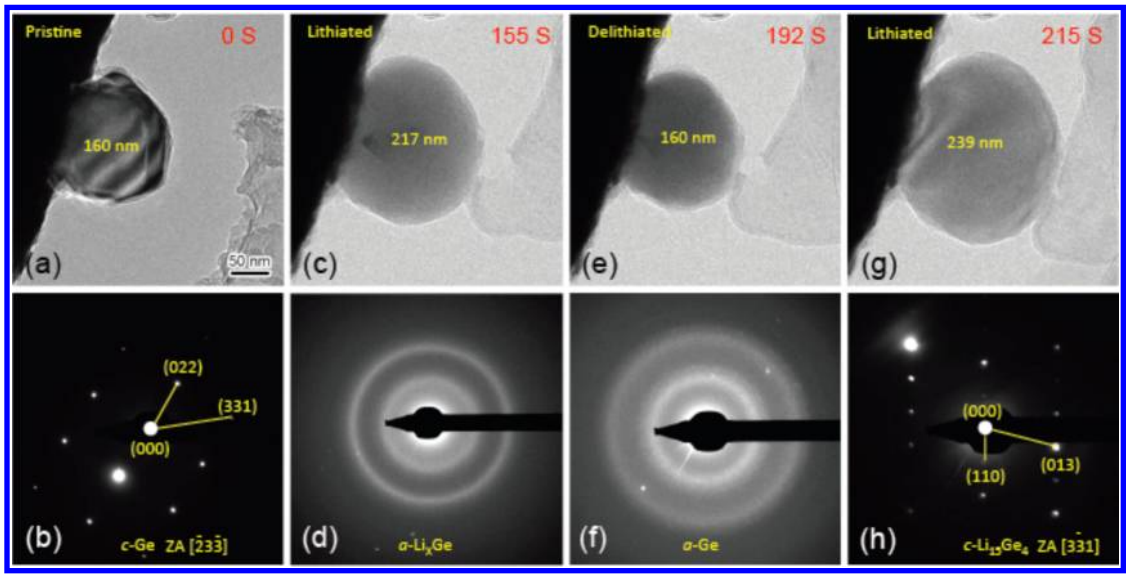

Figure 3. Identification of various crystalline or amorphous phases formed during lithiation delithiation cycling. (a) Pristine GeNP. (b) EDP showing that the pristine GeNP is single-crystalline. (c) Lithiated GeNP. (d) EDP showing that the amorphous lithiated phase is *a*-Li_xGe. (e) Fully delithiated GeNP. (f) EDP showing that the fully delithiated phase is *a*-Ge. (g) Fully lithiated GeNP. (h) EDP showing that the crystalline lithiated phase is *c*-$Li_{15}Ge_4$.

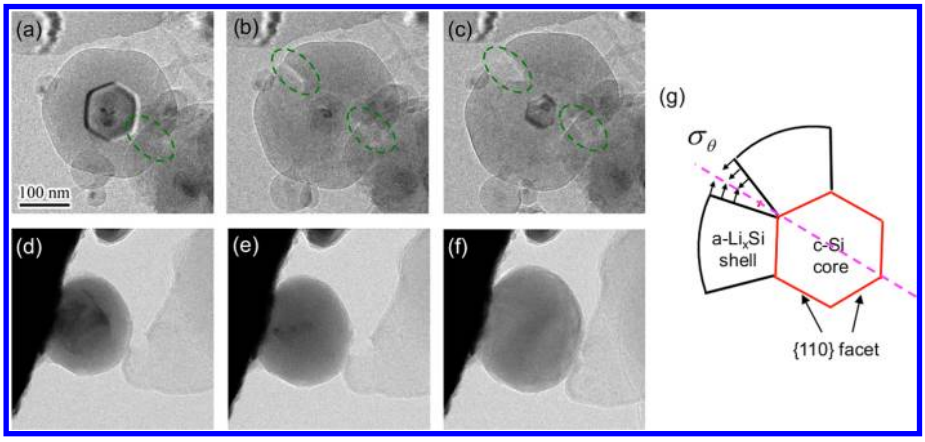

Figure 4. Lithiation-induced anisotropic swelling and fracture in a *c*-SiNP *versus* the isotropic swelling without fracture in a *c*-GeNP. The original sizes of both Si and Ge NPs are about 160 nm. (a) Partially lithiated SiNP showing the hexagon-shaped *c*-Si core with the {110} facets. (b,c) Fracture occurred in a late stage of lithiation. The well-defined fracture sites are indicated by green circles. (d,e) Partially lithiated GeNP showing the rounded *c*-Ge core. (f) Full lithiation without fracture of a GeNP. (g) Development of an intensified hoop tension near the fracture plane (indicated by the pink dashed line). When the anisotropic expansion occurs independently on each of {110} facets, a gap will form between the neighboring domains (black blocks) in the lithiated shell. To maintain the material coherency (by closing the gap), intensified hoop tension develops near the neighboring domains.

core shell structures in a partially lithiated SiNP (a) and GeNP (d). The original sizes of both NPs are around 160 nm. In the SiNP, the inner unlithiated core exhibits a hexagonal shape with {110} facets, which arises owing to the fastest lithiation rate of the {110} plane[25] in *c*-Si. The thickness of the lithiated shell is apparently orientation-dependent, further evidencing the strong anisotropy in swelling during lithiation. In contrast, lithiation in the GeNP is nearly orientation-independent, as manifested by the rounded core and the uniform thickness of the lithiated shell. The difference in the orientation dependence of lithiation in Si and Ge has a significant impact on their fracture behaviors, which will be further discussed next. Incidentally, the nearly isotropic lithiation in Ge is consistent with the much less anisotropic wet-etching rate in Ge than in Si.[23,24]

The most striking difference between SiNPs and GeNPs is their fracture behavior and cyclability. Our *in situ* TEM experiments have previously shown that the fracture of *c*-SiNPs is size-dependent; namely, above a threshold size of 150 nm in diameter, surface cracks nucleated and propagated in *c*-SiNPs upon the first lithiation.[7] In contrast, all of the GeNPs investigated in this work were tough without any visible crack-like defects formed even during multiple lithiation delithiation cycles. The fracture-free and electrochemically

cyclable features promise the GeNP as a robust, high-capacity anode material.

The tough behavior of the GeNPs is unexpected and ascribed to the isotropic nature of lithiation, as corroborated by our *in situ* TEM experiments and chemomechanical modeling. To appreciate the significance of such isotropy, it is essential to understand why the large *c*-SiNPs undergoing anisotropic swelling are fragile and why the *c*-GeNPs (with a wide size range of 100 nm to submicrometer) undergoing isotropic swelling are not. To address this question in a clear and complete manner, it is necessary to review the key understandings of fracture in lithiated nanoparticles and nanowires that have been recently advanced by our team and other groups. First, despite the compressive stress generated near the lithiation reaction front, the large lithiation-induced expansion occurring at the *curved* reaction front pushes out the material behind it, giving rise to a large hoop tension in the surface layer that drives the formation and propagation of surface cracks.[6 9] Second, when the particle size is small enough to be comparable to the surface flaw size, the driving force of surface cracking (*i.e.*, strain energy release rate) becomes dependent on the particle size.[7] Such a size-scaling explains the existence of the critical particle size above which fracture occurs upon lithiation.

While both the surface cracking and the size dependence of fracture have been rationalized, the effects of isotropic *versus* anisotropic lithiation on fracture are not accounted for in the aforementioned fracture analyses.[6 9] Here, we show that the lithiation isotropy turns out to be critical to the tough behavior of *c*-Ge, as opposed to the fragility of *c*-Si. In this regard, a key observation from the *in situ* TEM experiments of lithiation in *c*-SiNPs is the symmetry breaking of fracture in the circumferential direction. That is, fracture usually occurs on the well-defined angular site (indicated by green circles in Figure 4a c), which is located on one of the diameter planes (dashed line in Figure 4g) that passes through the opposite vertices of the hexagon-shaped *c*-Si core. Such well-defined fracture planes have also been reported in a recent experiment for *c*-SiNWs,[8] showing the fracture sites consistent with our observations. This characteristic fracture mode implies the existence of intensified hoop tension in these planes that likely originates from the anisotropic lithiation strain, as schematically illustrated in Figure 4g. At the respective {110} facets of the reaction front, the anisotropic lithiation strain could be dominated by the large expansion normal to the facets, resulting in a gap between the neighboring domains that are assumed to be lithiated independently. To maintain material coherency (*i.e.*, deformation compatibility), the large hoop tension arises near the interface plane of the neighboring domains in order to close the gap.

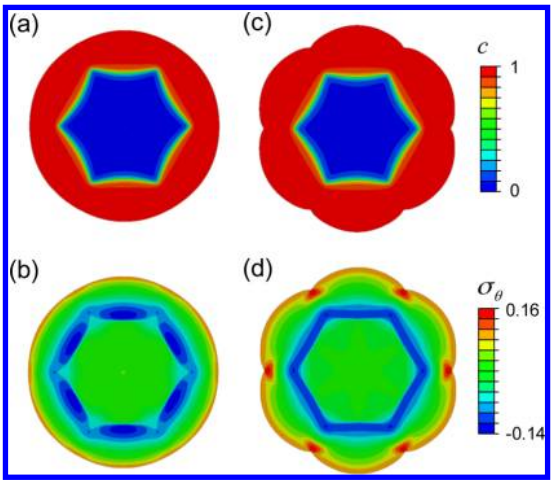

Figure 5. Chemomechanical modeling of the core shell structure and stress generation in the cross section of a lithiated nanowire, showing the effect of the anisotropy of lithiation strain: (a,b) $_{11}$ = $_{22}$ = 0.4; (c,d) $_{11}$ = 0.7 and $_{22}$ = 0.2. (a,c) Li concentration normalized by the maximum of $Li_{15}Si_4$, *c*. (b,d) Hoop stress normalized by Young's modulus, . A strong anisotropy of the lithiation strain can cause the intensified local hoop tension in the fracture plane observed in the TEM image in Figure 4.

To further appreciate the symmetry breaking of fracture in the circumferential direction as dictated by the anisotropy of lithiation strain, we invoke a recently developed continuum chemomechanical model[7,34] to simulate the concurrent processes of phase transformation and stress evolution during lithiation of a *c*-Si nanowire. The use of the nanowire geometry simplifies the analysis, while capturing the essential physics. In the model, a sharp reaction front with an abrupt change of the normalized Li concentration from zero (*c*-Si) to one (*a*-$Li_{15}Si_4$) is prescribed to move in the 110 direction.[7,34] The total strain $_{ij}$ consists of three parts, $_{ij}$ = $^{c}_{ij}$ $^{e}_{ij}$ $^{p}_{ij}$. That is, $^{c}_{ij}$ is the chemical strain given by $^{c}_{ij}$ = $_{ij}c$ (where *c* denotes the local normalized Li concentration and $_{ij}$ the expansion coefficient), $^{e}_{ij}$ is the elastic strain, and $^{p}_{ij}$ is the plastic strain. Here, the diagonal components of $_{ij}$ are allowed to take different values in the local coordinate system where the x_1 axis is aligned with the 110 direction (normal to the reaction front) and the x_2 axis is along the transverse direction of 112 . The assignment of anisotropic $_{ij}$ in our continuum model physically reflects the anisotropy of the lithiation strain that occurs at the sharp reaction front of {110} facets and computationally mediates the anisotropy of the total strain $_{ij}$, as dictated by the requirement of deformation compatibility. In Figure 5, we show the simulated Li distribution *c* (giving the core shell structure with {110} facets) and the associated hoop stress under two different assumptions for $_{ij}$ and accordingly different chemical strains of $^{c}_{ij}$: one is isotropic (with $_{11}$ = $_{22}$ = 0.4), and the other is anisotropic (with $_{11}$ = 0.7 and $_{22}$ = 0.2), and both give the same volume increase of 100%. In the former case (Figure 5b), the hoop tension is almost uniform along

the circumferential direction, which indicates that fracture, if occurred, would be possible at any surface location. Contrarily, non-uniform hoop tension develops in the latter case (Figure 5d), with intensified near the fracture planes observed in the experiments. Note that the above volume increase of 100% is smaller than that in the fully lithiated *c*-Si, but it facilitates numerical stability, while capturing the physical effect of anisotropic lithiation strain.

The highly anisotropic lithiation strain in *c*-Si is correlated with the orientation-dependent lithiation rate at the reaction front. While it has been unambiguously shown that lithiation of the {110} facet in *c*-Si involves the step-by-step ledge flow on the inclined, close-packed {111} layers,[25] it remains unclear as to what the exact local atomic arrangement of the Li_xSi product is on the Si{110} facet. The atomistic origin of anisotropic lithiation strain thus warrants further study in the future. At the continuum level, the lithiation strain should be generally larger in the normal direction than the tangential direction at the reaction front, owing to the constraint of the unlithiated core. However, considering the strong orientation dependence of the reaction rate in *c*-Si, it is conceivable that a strong anisotropy in the lithiation strain could possibly develop at the reaction front. On the other hand, given the orientation independence of the lithiation rate in *c*-Ge, the lithiation strain is expected to be more isotropic in *c*-Ge than in *c*-Si. As a result, the smaller anisotropy of the lithiation strain can effectively suppress the build-up of the high, non-uniform stress, giving rise to the tough response during the first lithiation of *c*-Ge and subsequent cycling of *a*-Ge, as well.

CONCLUSION

The electrochemical lithiation delithiation behavior of individual GeNPs was studied with *in situ* transmission electron microscopy. The results confirmed that the lithiation of GeNPs involves a two-step phase transformation: *a*-Ge → *a*-Li_xGe → *c*-$Li_{15}Ge_4$, with a total volume expansion of 260%, consistent with previous electrochemical tests. Fast multicycling of the GeNPs between the *a*-Ge and *a*-Li_xGe phases was demonstrated, with highly reversible expansion and contraction. In particular, our experiments demonstrated that the GeNPs with a wide size range (from 100 nm to submicrometers) remained robust without fracture in multiple cycles, in distinct contrast to the size-dependent fracture of SiNPs upon the first lithiation. Through a comparative study with fragile SiNPs, we conclude that the anisotropy of the lithiation strain causes the non-uniform stress in the hoop direction in lithiated SiNPs, leading to fracture in the well-defined planes. In the absence of such lithiation anisotropy, the *c*-GeNPs experience uniform hoop tension in the surface layer without the localized high stress and therefore remain robust throughout multicycling.

Our study of the anisotropic lithiation strain and fracture sheds new light onto the mitigation of electrochemically induced mechanical degradation in high-capacity electrode materials. Going beyond the crystalline Ge and Si and amorphous Ge studied herein, it can be reasoned that amorphous SiNPs or SiNWs should also remain robust upon lithiation because of their lack of crystallography-related anisotropy in the lithiation strain. Interestingly, this prediction is consistent with a recent experimental observation of cycling of amorphous SiNPs without fracture.[35] Eliminating the anisotropy of the lithiation strain by amorphization[36] thus presents a novel pathway to mitigate the mechanical degradation in high-capacity electrode materials. In addition, we note that a lithiation delithiation cycle is completed in a few minutes in our experiments, which is much faster than the typical charging discharging rate for conventional battery cells. Nevertheless, the effect of the cycling rate on fracture warrants systematic study in the future. Finally, we stress that, while the intrinsic tough behavior of GeNPs facilitates the electrode integrity, maintaining a stable solid electrolyte interphase (SEI) during large-strain electrochemical cycling remains an outstanding challenge in the application of high-capacity anodes for Li-ion batteries.

METHODS

In our *in situ* TEM experiments, the GeNPs (or SiNPs) were used as the working electrode; the Li metal on a tungsten (W) probe was the counter electrode, and a native lithium oxide (Li_2O) layer acted as a solid-state electrolyte (Figure 1c). The Li_2O/Li electrode was driven by a piezo-positioner (Nanofactory, TEM STM holder) to contact the GeNPs (or SiNPs), and then a bias of 2 V (1 V) was applied to the Pt rod with respect to the W rod to initiate and sustain the lithiation (delithiation).

Conflict of Interest: The authors declare no competing financial interest.

Acknowledgment. The support by the NSF Grants CMMI-1100205 and 1201058 is greatly acknowledged. Portions of this work were supported by a Laboratory Directed Research and Development (LDRD) project at Sandia National Laboratories (SNL) and partly by Nanostructures for Electrical Energy Storage (NEES), an Energy Frontier Research Center (EFRC) funded by the U.S. Department of Energy, Office of Science, Office of Basic Energy Sciences under Award Number DESC0001160. The LDRD supported the development and fabrication of platforms. The NEES center supported the development of TEM techniques. CINT supported the TEM capability; in addition, this work represents the efforts of several CINT users, primarily those with affiliation external to Sandia National Laboratories. In addition, this work was performed, in part, at the Sandia-Los Alamos Center for Integrated Nanotechnologies (CINT), a U.S. Department of Energy, Office of Basic Energy Sciences user facility. Sandia National Laboratories is a multiprogram laboratory operated by Sandia Corporation, a wholly owned subsidiary of Lockheed Martin Company, for the U.S. Department of Energy's

National Nuclear Security Administration under contract DE-AC04-94AL85000.

Supporting Information Available: Supporting movie showing the lithiation/delithiation behaviors of GeNPs and SiNPs. This material is available free of charge *via* the Internet at http://pubs.acs.org.

REFERENCES AND NOTES

1. Tarascon, J. M.; Armand, M. Issues and Challenges Facing Rechargeable Lithium Batteries. *Nature* 2001, *414*, 359 367.
2. Arico, A. S.; Bruce, P.; Scrosati, B.; Tarascon, J.-M.; van Schalkwijk, W. Nanostructured Materials for Advanced Energy Conversion and Storage Devices. *Nat. Mater.* 2005, *4*, 366 377.
3. Service, R. F. Getting There. *Science* 2011, *332*, 1494 1496.
4. Huggins, R. A.; Nix, W. D. Decrepitation Model for Capacity Loss during Cycling of Alloys in Rechargeable Electrochemical Systems. *Ionics* 2000, *6*, 57 63.
5. Beaulieu, L. Y.; Eberman, K. W.; Turner, R. L.; Krause, L. J.; Dahn, J. R. Colossal Reversible Volume Changes in Lithium Alloys. *Electrochem. Solid State Lett.* 2001, *4*, A137 A140.
6. Liu, X. H.; Zheng, H.; Zhong, L.; Huang, S.; Karki, K.; Zhang, L. Q.; Liu, Y.; Kushima, A.; Liang, W. T.; Wang, J. W.; *et al.* Anisotropic Swelling and Fracture of Silicon Nanowires during Lithiation. *Nano Lett.* 2011, *11*, 3312 3318.
7. Liu, X. H.; Zhong, L.; Huang, S.; Mao, S. X.; Zhu, T.; Huang, J. Y. Size-Dependent Fracture of Silicon Nanoparticles during Lithiation. *ACS Nano* 2012, *6*, 1522 1531.
8. Lee, S. W.; McDowell, M. T.; Berla, L. A.; Nix, W. D.; Cui, Y. Fracture of Crystalline Silicon Nanopillars during Electrochemical Lithium Insertion. *Proc. Natl. Acad. Sci. U.S.A.* 2012, *109*, 4080 4085.
9. Zhao, K. J.; Pharr, M.; Wan, Q.; Wang, W. L.; Kaxiras, E.; Vlassak, J. J.; Suo, Z. G. Concurrent Reaction and Plasticity during Initial Lithiation of Crystalline Silicon in Lithium-Ion Batteries. *J. Electrochem. Soc.* 2012, *159*, A238 A243.
10. He, Y.; Yu, X.; Li, G.; Wang, R.; Li, H.; Wang, Y.; Gao, H.; Huang, X. Shape Evolution of Patterned Amorphous and Polycrystalline Silicon Microarray Thin Film Electrodes Caused by Lithium Insertion and Extraction. *J. Power Sources* 2012, *216*, 131 138.
11. He, Y.; Yu, X.; Wang, Y.; Li, H.; Huang, X. Alumina-Coated Patterned Amorphous Silicon as the Anode for a Lithium-Ion Battery with High Coulombic Efficiency. *Adv. Mater.* 2011, *23*, 4938 4941.
12. Guo, J.; Sun, A.; Chen, X.; Wang, C.; Manivannan, A. Cyclability Study of Silicon-Carbon Composite Anodes for Lithium-Ion Batteries Using Electrochemical Impedance Spectroscopy. *Electrochim. Acta* 2011, *56*, 3981 3987.
13. Liu, X. H.; Liu, Y.; Kushima, A.; Zhang, S. L.; Zhu, T.; Li, J.; Huang, J. Y. *In Situ* TEM Experiments of Electrochemical Lithiation and Delithiation of Individual Nanostructures. *Adv. Energy Mater.* 2012, *2*, 722 741.
14. Kasavajjula, U.; Wang, C. S.; Appleby, A. J. Nano- and Bulk-Silicon-Based Insertion Anodes for Lithium-Ion Secondary Cells. *J. Power Sources* 2007, *163*, 1003 1039.
15. Larcher, D.; Beattie, S.; Morcrette, M.; Edstroem, K.; Jumas, J.-C.; Tarascon, J.-M. Recent Findings and Prospects in the Field of Pure Metals as Negative Electrodes for Li-Ion Batteries. *J. Mater. Chem.* 2007, *17*, 3759 3772.
16. Graetz, J.; Ahn, C. C.; Yazami, R.; Fultz, B. Nanocrystalline and Thin Film Germanium Electrodes with High Lithium Capacity and High Rate Capabilities. *J. Electrochem. Soc.* 2004, *151*, A698 A702.
17. Chan, C. K.; Zhang, X. F.; Cui, Y. High Capacity Li Ion Battery Anodes Using Ge Nanowires. *Nano Lett.* 2008, *8*, 307 309.
18. Lee, H.; Kim, H.; Doo, S. G.; Cho, J. Synthesis and Optimization of Nanoparticle Ge Confined in a Carbon Matrix for Lithium Battery Anode Material. *J. Electrochem. Soc.* 2007, *154*, A343 A346.
19. Jo, G.; Choi, I.; Ahn, H.; Park, M. J. Binder-Free Ge Nanoparticles-Carbon Hybrids for Anode Materials of Advanced Lithium Batteries with High Capacity and Rate Capability. *Chem. Commun.* 2012, *48*, 3987 3989.
20. Xue, D. J.; Xin, S.; Yan, Y.; Jiang, K. C.; Yin, Y. X.; Guo, Y. G.; Wan, L. J. Improving the Electrode Performance of Ge through Ge@C Core Shell Nanoparticles and Graphene Networks. *J. Am. Chem. Soc.* 2012, *134*, 2512 2515.
21. Park, M. H.; Cho, Y.; Kim, K.; Kim, J.; Liu, M. L.; Cho, J. Germanium Nanotubes Prepared by Using the Kirkendall Effect as Anodes for High-Rate Lithium Batteries. *Angew. Chem., Int. Ed.* 2011, *50*, 9647 9650.
22. Liu, X. H.; Huang, S.; Picraux, S. T.; Li, J.; Zhu, T.; Huang, J. Y. Reversible Nanopore Formation in Ge Nanowires during Lithiation Delithiation Cycling: An *In Situ* Transmission Electron Microscopy Study. *Nano Lett.* 2011, *11*, 3991 3997.
23. Leancu, R.; Moldovan, N.; Csepregi, L.; Lang, W. Anisotropic Etching of Germanium. *Sens. Actuators, A* 1995, *46*, 35 37.
24. Schwartz, B. Chemical Etching of Germanium in the System $HF-H_2O_2-H_2O$. *J. Electrochem. Soc.* 1967, *114*, 285 292.
25. Liu, X. H.; Wang, J. W.; Huang, S.; Fan, F.; Huang, X.; Liu, Y.; Krylyuk, S.; Yoo, J.; Dayeh, S. A.; Davydov, A. V.; *et al. In Situ* Atomic-Scale Imaging of Electrochemical Lithiation in Silicon. *Nat. Nanotechnol.* 2012, *7*, 749 756.
26. Huang, J. Y.; Zhong, L.; Wang, C. M.; Sullivan, J. P.; Xu, W.; Zhang, L. Q.; Mao, S. X.; Hudak, N. S.; Liu, X. H.; Subramanian, A.; *et al. In Situ* Observation of the Electrochemical Lithiation of a Single SnO_2 Nanowire Electrode. *Science* 2010, *330*, 1515 1520.
27. Liu, Y.; Zheng, H.; Liu, X. H.; Huang, S.; Zhu, T.; Wang, J.; Kushima, A.; Hudak, N. S.; Huang, X.; Zhang, S.; *et al.* Lithiation-Induced Embrittlement of Multiwalled Carbon Nanotubes. *ACS Nano* 2011, *5*, 7245 7253.
28. Liu, X. H.; Zhang, L. Q.; Zhong, L.; Liu, Y.; Zheng, H.; Wang, J. W.; Cho, J.-H.; Dayeh, S. A.; Picraux, S. T.; Sullivan, J. P.; *et al.* Ultrafast Electrochemical Lithiation of Individual Si Nanowire Anodes. *Nano Lett.* 2011, *11*, 2251 2258.
29. Liu, X. H.; Fan, F.; Yang, H.; Zhang, S.; Huang, J. Y.; Zhu, T. Self-Limiting Lithiation in Silicon Nanowires. *ACS Nano* 2013, *7*, 1495 1503.
30. Obrovac, M. N.; Krause, L. J. Reversible Cycling of Crystalline Silicon Powder. *J. Electrochem. Soc.* 2007, *154*, A103 A108.
31. Johnson, Q.; Smith, G. S.; Wood, D. Crystal Structure of $Li_{15}Ge_4$. *Acta Crystallogr.* 1965, *18*, 131 &.
32. Wang, C.-M.; Li, X.; Wang, Z.; Xu, W.; Liu, J.; Gao, F.; Kovarik, L.; Zhang, J.-G.; Howe, J.; Burton, D. J.; *et al. In Situ* TEM Investigation of Congruent Phase Transition and Structural Evolution of Nanostructured Silicon/Carbon Anode for Lithium Ion Batteries. *Nano Lett.* 2012, *12*, 1624 1632.
33. McDowell, M. T.; Ryu, I.; Lee, S. W.; Wang, C.; Nix, W. D.; Cui, Y. Studying the Kinetics of Crystalline Silicon Nanoparticle Lithiation with *In Situ* Transmission Electron Microscopy. *Adv. Mater.* 2012, *24*, 6034 6041.
34. Yang, H.; Huang, S.; Huang, X.; Fan, F. F.; Liang, W. T.; Liu, X. H.; Chen, L. Q.; Huang, J. Y.; Li, J.; Zhu, T.; *et al.* Orientation-Dependent Interfacial Mobility Governs the Anisotropic Swelling in Lithiated Silicon Nanowires. *Nano Lett.* 2012, *12*, 1953 1958.
35. McDowell, M. T.; Lee, S. W.; Harris, J. T.; Korgel, B. A.; Wang, C.; Nix, W. D.; Cui, Y. *In Situ* TEM of Two-Phase Lithiation of Amorphous Silicon Nanospheres. *Nano Lett.* 2013, *13*, 758 764.
36. Wang, J. W.; He, Y.; Fan, F.; Liu, X. H.; Xia, S.; Liu, Y.; Harris, C. T.; Li, H.; Huang, J. Y.; Mao, S. X.; *et al.* Two-Phase Electrochemical Lithiation in Amorphous Silicon. *Nano Lett.* 2013, *13*, 709 715.